Vertical Flux of Energy into the Lower Ionosphere from Internal Gravity Waves Generated in the Troposphere

EARL E. GOSSARD

U. S. Navy Electronics Laboratory, San Diego, California

Abstract. It has been suggested by C. O. Hines that internal atmospheric gravity waves may account for many of the irregularities observed in the lower ionosphere and that these waves may have their origin in the large energy regions of the lower troposphere. The problem of vertical energy flow in the gravity-wave range of the atmospheric spectrum is examined in the present paper. Observational data on tropospheric internal waves are used to compute the energy density spectra and the spectra of vertical energy flux. It is found that a window can exist at periods of about 10 minutes to 2 hours through which fairly large amounts of energy sometimes flow out of the troposphere. Observational data at *D*-layer and meteor heights are compared with observations of tropospheric internal waves.

Introduction. It has been suggested by *Hines* [1960] that much of the observational data on irregularities in the ionosphere can be interpreted in terms of internal atmospheric gravity waves. Since there is no obvious mechanism for generating waves at these levels other than low-frequency tidal forces, Hines suggests that they may have their origin in the large energy processes of the troposphere.

Recently *Charney and Drazin* [1961] performed a theoretical study of the flow of energy out of the troposphere from planetary scale disturbances. They found that most of the energy is confined to the troposphere and stratosphere by the increase of wind speed with height, and a large vertical flux of energy at these frequencies appears to be possible only during the equinoctial periods when the flow aloft is reversing its direction.

In this paper we intend to examine the vertical flux of energy out of the lower troposphere at frequencies and scale sizes characteristic of internal gravity waves and to compare the results with data on the lower ionosphere obtained by *Hargreaves* [1961], *Greenhow and Neufeld* [1959], and others.

Description of tropospheric internal waves. Internal waves in the troposphere have been observed in southern California for many years [*Gossard and Munk,* 1954], and the data which have been collected can be used to obtain the energy density spectrum and the vertical energy flux. The observations, illustrated by Figure 1, were recorded at the U. S. Navy Electronics Laboratory (NEL). The transducer used for the pressure record is essentially a microphone with slow leaks of different rates into chambers on opposite sides of a diaphragm. Deflection of a diaphragm varies the capacitance in one arm of a capacitance bridge whose output is then amplified and recorded. This system has been described by *Johnson and Chiles* [1957].

Figure 1 illustrates several significant features of these tropospheric waves. The period of the waves is directly available from the records, although it sometimes has to be corrected for Doppler shift due to the mean drift of the medium. The direction and speed of the particle motion within the wave is also directly available from the records, and therefore the direction of propagation can be obtained from simple vector diagrams. Furthermore, since both pressure and wind speed are directly observable, the phase velocity of the waves is observable also since the phase velocity C of the waves relative to the airstream is given by

$$C = p/\rho v \qquad (1)$$

where p is the pressure perturbation of the waves, v is the horizontal wind speed perturbation, and ρ is the density. If the wave train is imbedded in a moving airstream, the phase velocity relative to a fixed observer should be corrected for the ambient velocity of the airstream. This method of obtaining phase velocity, wavelength and direction of propagation has been described in detail by *Gossard and Munk* [1954]. The important thing to note here is that

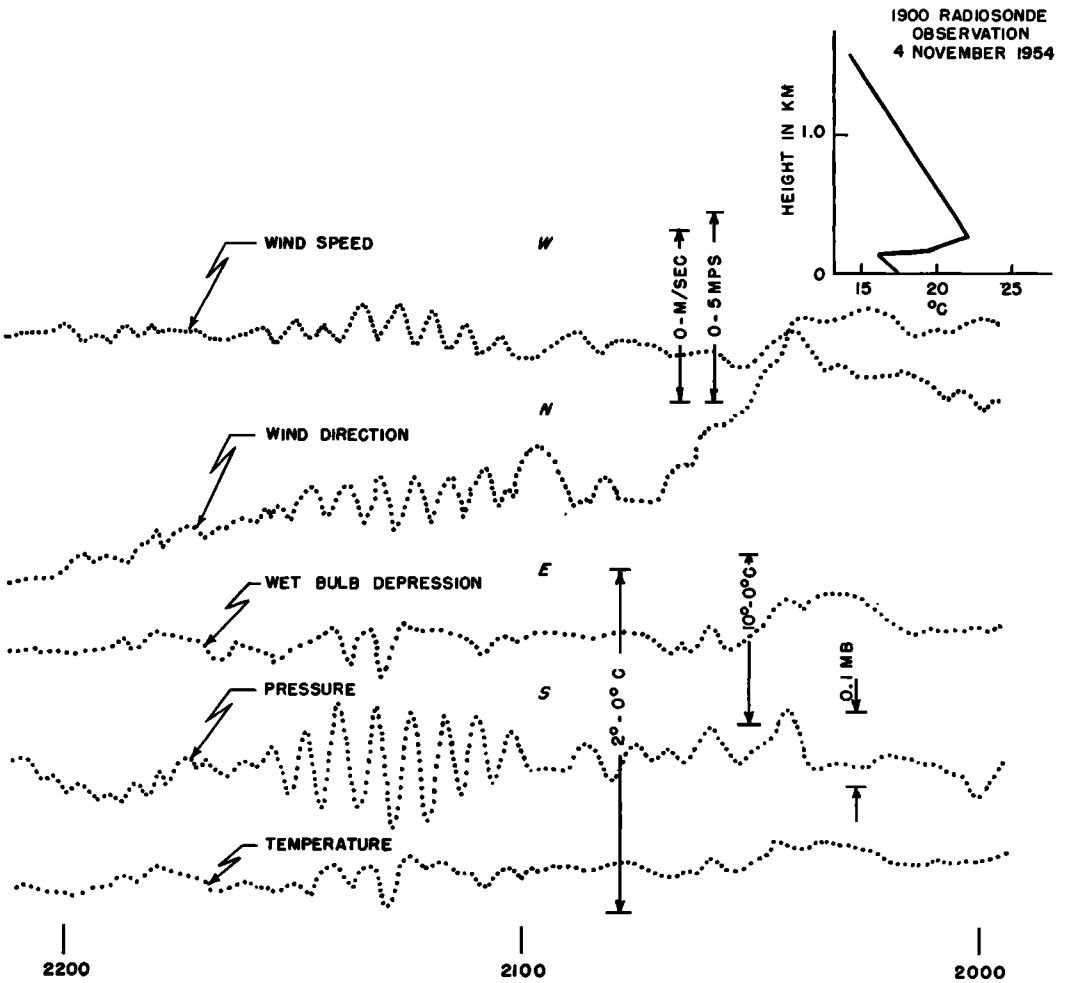

Fig. 1. Surface pressure record of November 4, 1954. Temperature and wet-bulb depression increase downwards.

phase velocity, wavelength, and direction of propagation are all observable quantities.

Under special conditions the waves may be visible on cloud formations, although it is very doubtful that the usual billow-cloud rolls are true gravity waves. There are many famous photographs of cloud formations in the waves in the lee of mountains, but true examples of free progressive wave trains are rare. Figure 2 shows photographs of the effect of a wave train on a fog layer, and Figure 3 shows the corresponding records of wind and surface pressure.

The bank of fog about 500 feet thick lay south of Point Loma, California (from which the photographs of Figure 2 were taken), during passage of the main wave train. The waves are shown as perturbations of the top of the fog bank. By the time photographs could be taken the waves were considerably reduced in amplitude though still clearly visible. Their period and general direction of propagation can be estimated by relating the time the pictures were taken to the position of the waves (such as wave B for example) with respect to landmarks in the foreground. Note that even these relatively high frequency waves (about 7 minute period) are very prominent on the cirrus cloud deck high in the troposphere.

Records of the type so far described indicate that typical phase velocities are 10 to 25 m/sec.

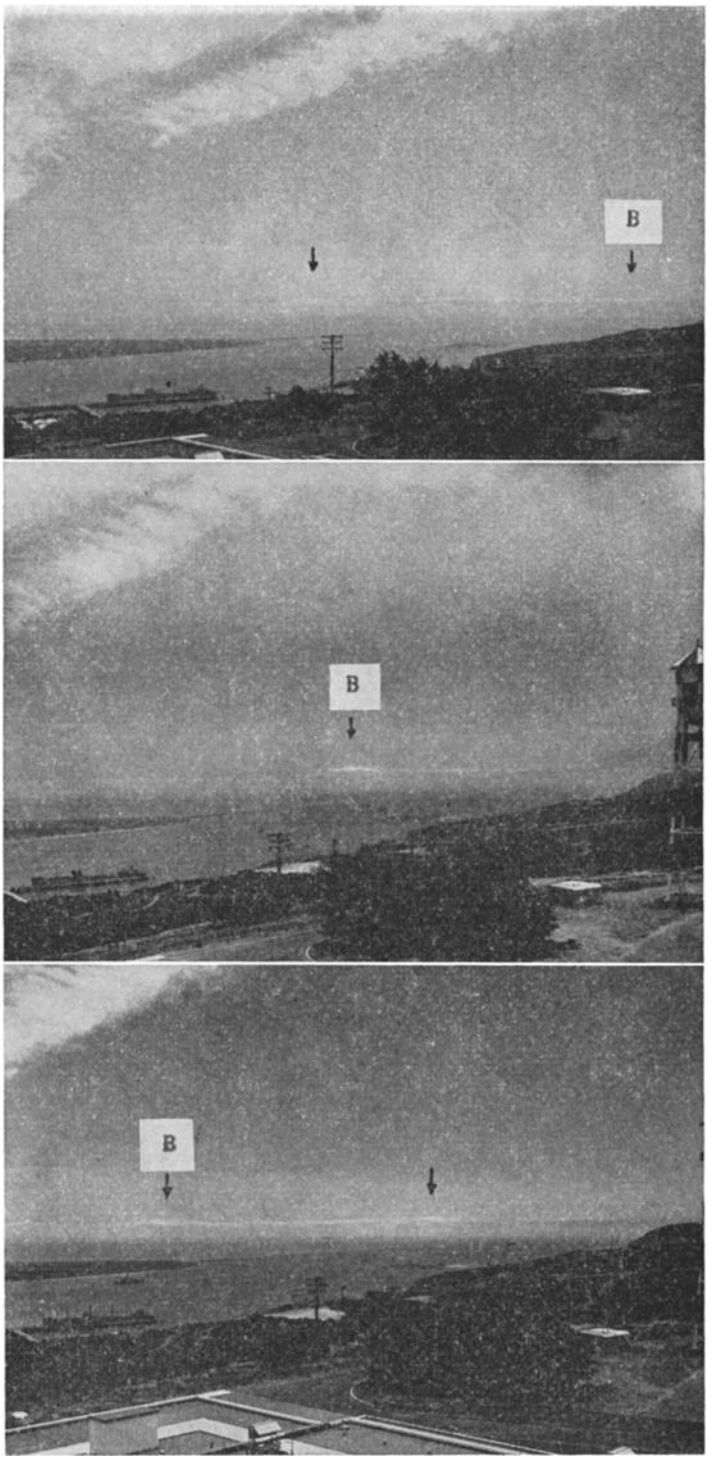

Fig. 2. Photographs of internal waves perturbing top of fog layer. Arrows indicate wave crests. Note that large perturbations extend through the cirrus cloud level. Top picture taken at 1137 PST, middle picture at 1144, bottom picture at 1149.

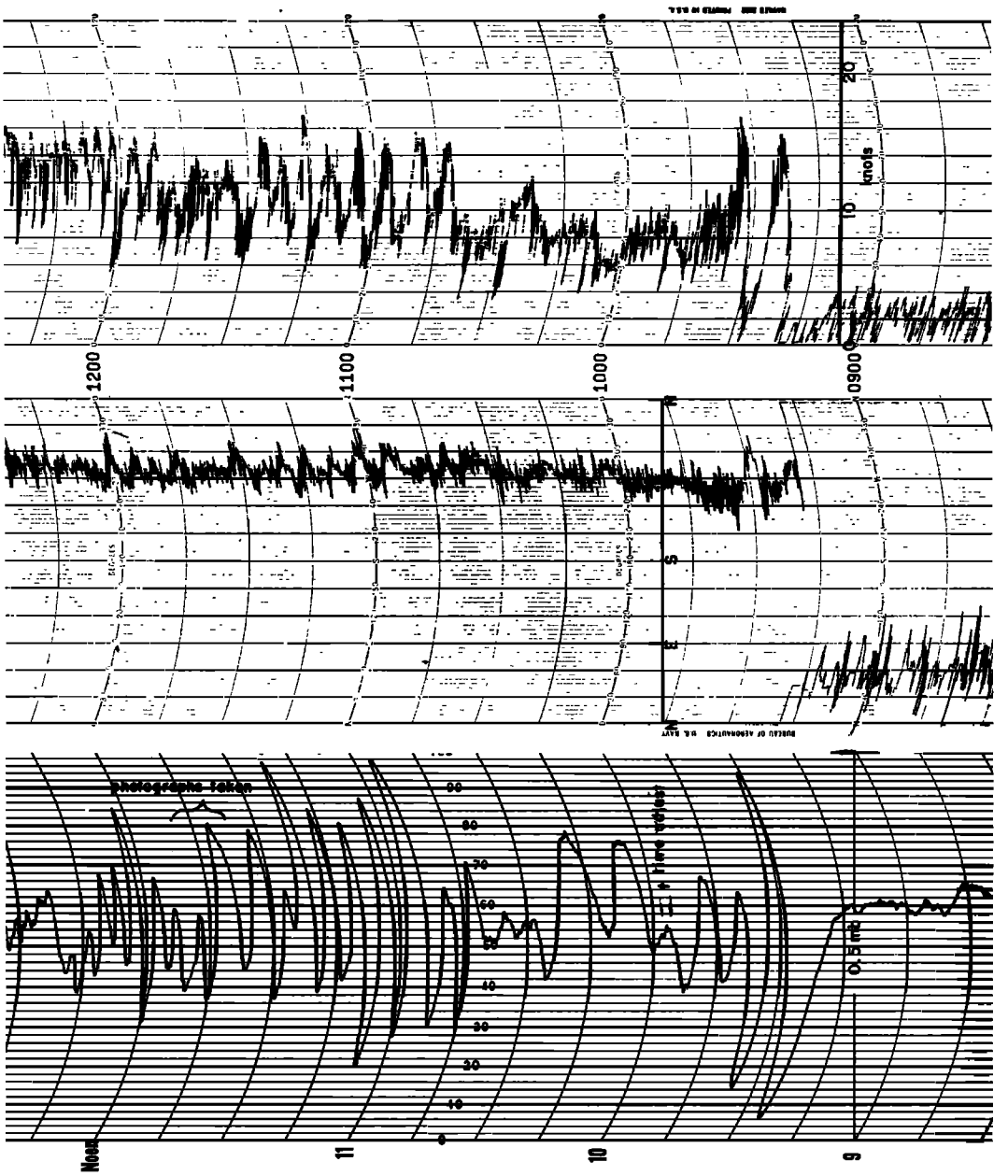

Fig. 3. Record of surface pressure and wind of May 19, 1955. Record shows the wave train whose photographs are shown in Figure 2.

Typical wave periods are 5 minutes to more than an hour. Often a fairly narrow spectral band at periods of 7 to 12 minutes is present, giving the records a nearly sinusoidal character. This band is especially prominent when the waves have traveled some distance from the region of generation, allowing energy in the lower-frequency components to leak into the upper atmosphere. Near the source region the low-frequency components are quite prominent, and the records have an erratic appearance. The fluctuations sometimes continue for as long

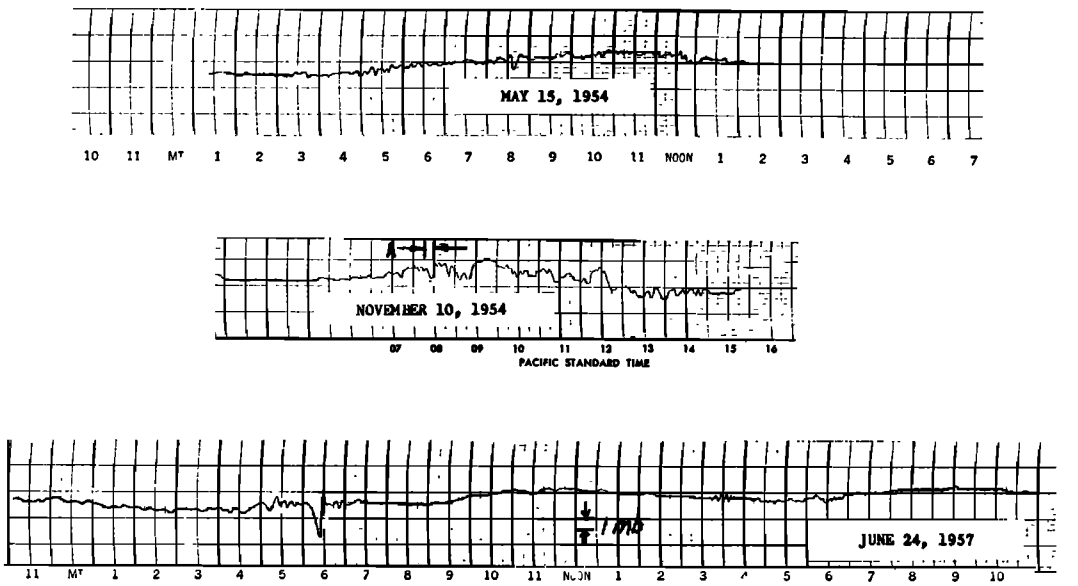

Fig. 4. Microbarograph records showing internal wave activity. These records are from a conventional microbarograph whose sensitivity has been increased. A pilot balloon observation was taken through wave A of November 10.

as 10 to 12 hours, and such records are often suitable for statistical analysis. We have used them to compute the energy density spectrum and the spectrum of vertical energy flux out of the lower troposphere. Some examples of records so analyzed are shown in Figure 4, in which records from a conventional barograph with increased sensitivity illustrate the over-all appearance of the fluctuation records. The records actually used in the spectrum analyses were recorded with the barovariograph described above and with a sensitive absolute-pressure-measuring system at the Scripps Institution of Oceanography as described by Gossard and Munk.

In the geographical area where the measurements were made, the temperature distribution in the lower atmosphere is often characterized by a very stable layer (an abrupt density decrease) 1000 to 5000 feet above the surface. Below the layer the temperature distribution is usually almost adiabatic. Above the layer the temperature gradient is somewhat less than adiabatic, and the exact distribution of entropy (or potential temperature) above the stable layer is very important because it determines the amount and spectral distribution of the energy 'leaking' out of the lower troposphere owing to internal waves. The distribution of potential temperature within the layers is conveniently described in terms of the Vaisala (or Brunt) frequency N, defined as

$$N = \left[g \frac{d}{dz} (\ln \theta) \right]^{1/2} \tag{2}$$

where g is the acceleration of gravity, θ is potential temperature, and N is identical with s used by Gossard and Munk. This very important parameter has been discussed in detail by *Eckart* [1960]. The distribution of θ with height on June 24, 1957, and May 15, 1954, is shown in Figure 5.

The model of the troposphere. The eigensolution for a three-layer model atmosphere can be obtained without difficulty when N is constant within each layer. However, for the purposes of the present discussion, a simpler model will be adopted which retains the essential features of the more complete model but allows a more simple discussion of the untrapped portion of the spectrum. For the moment a discontinuity will be assumed between a nearly adiabatic lower layer and a relatively warm upper layer. Below the layer the gradient of the logarithm of potential temperature is described by N_1, and above the layer it is described by N_3.

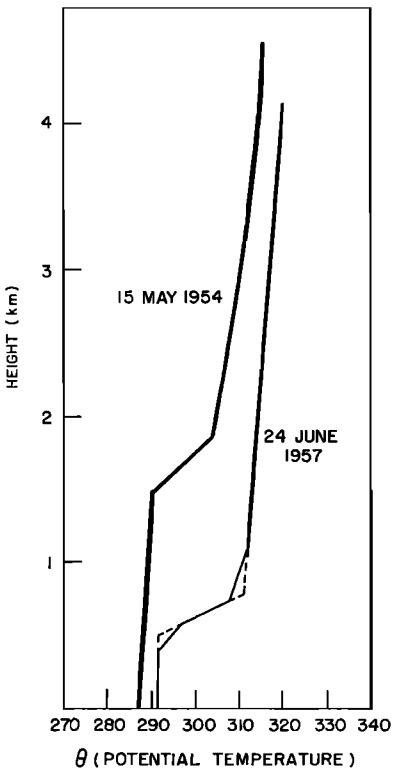

Fig. 5. Radiosonde observations for 0700 PST, May 15, 1954, and 0400 PST, June 24, 1957. Potential temperature θ is $T(1000/p)^{0.286}$.

The derivation of the equations will be given later, but we state now that the frequency equation is given by

$$\left(\frac{\omega}{k}\right)^2 = \frac{gH\ \Delta \ln \theta}{\gamma_1 H \coth \gamma_1 H + \gamma_3 H} \cong \frac{gH\ \Delta \ln \theta}{1 + \gamma_3 H} \qquad \gamma_1 H \ll 1.0 \qquad (3)$$

where k is the horizontal component of the wave number, ω is the angular frequency, H is the height of the discontinuity, and $\gamma_{1,3}$ is approximately $k[1 - (N_{1,3}/\omega)^2]^{1/2}$. Equation 3 shows that k must be complex for frequencies less than N_3, and the waves are attenuated with distance owing to leakage of energy into the upper atmosphere. The attenuation coefficient k_i is shown as a function of frequency in Figure 6. The maximum leakage into the upper atmosphere occurs at periods of 12 to 20 minutes if we start with a white energy density spectrum. However, the energy spectrum is not white and must be obtained experimentally. Sensitive measurements of surface pressure can provide the observational data required if the wavelengths are long enough ($k\,H$ small enough) to cause appreciable pressure perturbations at the earth's surface. It is the untrapped frequencies (γ_3 imaginary) with which we shall be concerned, since energy at these frequencies may be propagated into the upper atmosphere. For these frequencies the problem is indeterminate. However, if the fluid is considered to be (negligibly) viscous and if no energy is reflected from the ionosphere, physically meaningful solutions can be obtained. These are reasonable assumptions because the rapid increase in kinematic viscosity in the lower ionosphere would lead to viscous attenuation (especially of the higher frequencies), and because the growth of amplitude with decreasing density shown by equation 4 would cause the larger waves to become nonlinear at some height and deposit their energy in the turbulence spectrum.

For our model the displacement amplitude η below H is given by

$$\eta = \eta_H \left(\frac{\rho_H}{\rho_z}\right)^{1/2} \frac{\sinh \gamma_1 z}{\sinh \gamma_1 H} \qquad (4)$$

where ρ_z is the density at height z, ρ_H is the density at H, and η_H is the amplitude of the displacement at H. η_H is related to the surface pressure by[1]

$$\eta_H = (\rho_0 \rho_H)^{-1/2} \cdot \frac{\cosh \gamma_1 H + (\gamma_3/\gamma_1) \sinh \gamma_1 H}{g\ \Delta \ln \theta}\, p(0) \qquad (5)$$

where $p(0)$ is the surface pressure perturbation. The total external energy density is given for these waves by the sum of their kinetic and thermobaric energies [for example, see *Eckart*, 1960]. Immediately above a thin stable layer the energy density ϵ is therefore given by

$$\epsilon = \tfrac{1}{2}\rho_z(|\mathbf{v}|^2 + N^2\,|\eta|^2) \qquad (6)$$

where $|\mathbf{v}|^2$ is the square of the modulus of the complex velocity perturbation vector. The

[1] For the frequency band near N_3 which is prominent on most of the records $\gamma_3 \cong 0$. Equation 5 then reduces to $\eta_H \cong p(0)\ (\cosh \gamma_1 H/\rho_0 g \Delta \ln \theta)$ as given by *Gossard* [1960]. For the present problem a wide range of the spectrum is considered and equation 5 must be used.

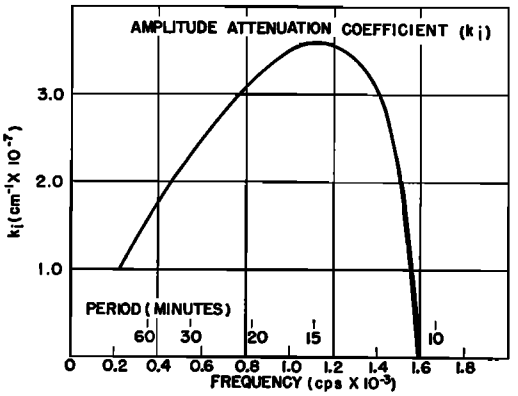

Fig. 6. Amplitude attenuation coefficient calculated from equation 25 assuming an adiabatic surface layer and $gH\Delta \ln \theta = 67$. Frequency in cycles/kilosecond.

vertical energy flux J_z is given by

$$J_z = 1/2(pw^* + p^*w) \qquad (7)$$

where p^* and w^* are the complex conjugates of pressure and vertical velocity.

Results. The energy density spectra for the records of Figure 4 are shown in Figure 7. The tropospheric sounding data show the trapping period[2] to be about 10 minutes on June 24, 1957, and 7 minutes on May 15, 1954.

The total energy density in the spectra was 0.73 erg/cm³ in the morning and 0.03 erg/cm³ in the afternoon of June 24, 1957. On May 15 the energy density was 0.78 erg/cm³ and on November 10, 3.2 ergs/cm³.

The corresponding spectra of vertical energy flux are shown in Figure 8. A maximum in vertical energy flux occurs at frequencies whose periods range from 7.5 minutes to 2 hours as was suggested by the form of the attenuation coefficient k_i. The total energy flow represented by these spectra is fairly large. It was 472 ergs/cm² sec on June 24 (A.M.), 18 ergs/cm² sec on June 24 (P.M.), and 677 ergs/cm² on May 15. The computed energy flux out of the lower troposphere for November 10, is very large (964 ergs/cm² sec). However, the temperature sounding shows an adiabatic layer higher in the troposphere on this day, and most of the energy must have been reflected at this level. For this reason the spectrum of vertical energy flux for November 10 is probably not realistic and is not shown.

Apparently the vertical energy flow can amount to as much as 1000 ergs/cm² sec. This is seen to be fairly large when compared with the total rate of turbulent dissipation of energy in a unit column of atmosphere which is about 4500 ergs/cm² sec. Records of wave activity as prominent as those shown are rare, occurring only a few times a year in southern California. However, an energy flux of 50 to 100 ergs/cm² sec is associated with many storms and frontal systems.

Several factors have not been taken into account in the present analysis:

1. Viscosity has been neglected. Although the effects of molecular viscosity below 60 km are

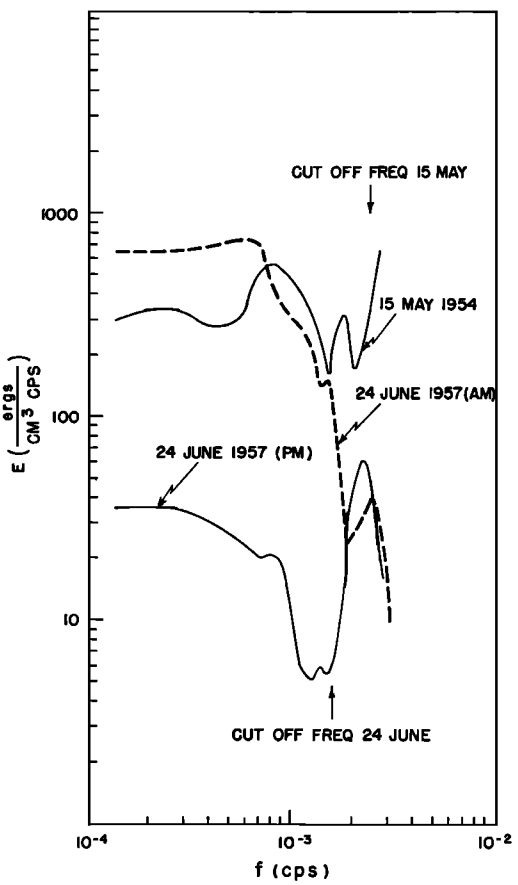

Fig. 7. Energy density spectra above the temperature inversion on May 15, 1954, and June 24, 1957.

[2] Trapping or cutoff frequency is used here as the frequency at which J_z becomes zero in the region above the stable layer.

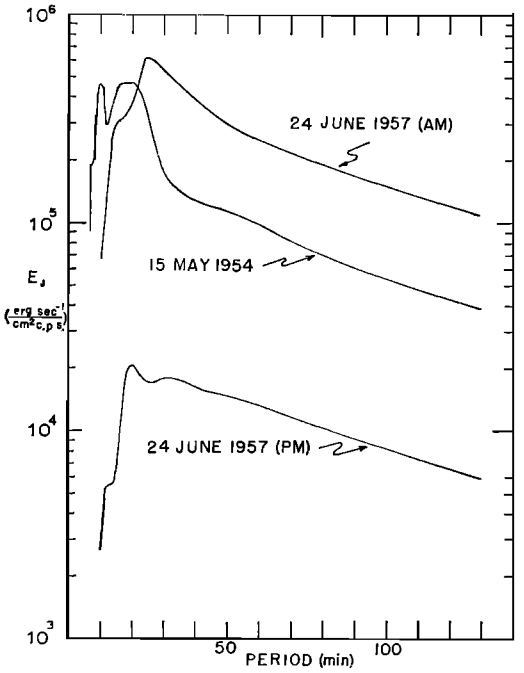

Fig. 8. Vertical flux of energy out of the lower troposphere on May 15, 1954, and June 24, 1957.

negligible, the values of the turbulent viscosity coefficient may become quite large and cause some attenuation in the stratosphere and upper troposphere.

2. The effects of shearing layers have not been considered. Under some conditions wind shear could cause the waves to be reflected or to become unstable before reaching the ionosphere.

3. The nonlinear terms in the equations of motion have been neglected. The perturbation equations have been used to obtain solutions in which small amplitude ($k\eta \ll 1.0$) fluctuations are assumed. However, we see from (4) that the displacement amplitude η is proportional to $\rho_z^{-1/2}$ and can therefore become very large when the density ρ_z becomes very small. The resulting nonlinearity could cause the waves (especially the shorter wavelengths) to deposit their energy in the turbulence spectrum before reaching the ionosphere.

Comparison with ionospheric data. Although three of the records analyzed above must be considered as representing exceptionally disturbed conditions, the record on the afternoon of June 24, 1957, is fairly typical of the activity to be expected in the untrapped frequencies of the spectrum. This is supported by the spectrum of surface pressure from periods of 0.2 second to 1 week given by *Gossard* [1960] on the basis of many samples of surface pressure data. It is therefore of interest to compare the statistics of the afternoon record of June 24 with observational data from the lower ionosphere. On this day, maximum vertical energy flow was associated with periods of 26 minutes,[3] and approximately 90 per cent of the total flux occurred between periods of 15 minutes and 2 hours. The rms amplitude fluctuation was 9 meters, and the rms wind speed fluctuation was 12 cm/sec. If these figures are converted to the corresponding values at 80 km, using values of atmospheric density from the U. S. A. F. *Handbook of Geophysics* [1960], the amplitude perturbation is about 2 km and the rms wind speed perturbation is 29 m/sec. The horizontal phase velocity of the waves on June 24 was 21 m/sec. The horizontal wavelength for waves of 15-minute period was 19 km and for waves of 2-hour period it was 150 km. It will be shown that the vertical wavelength λ_z of the untrapped waves can be estimated from

$$\lambda_z \cong 2\pi C(N_{80}^2 - \omega^2)^{-1/2} \qquad (8)$$

where C is the phase velocity and N_{80} is the Vaisala frequency at 80 km. N_{80} is approximately 0.02 rad/sec, which is much greater than ω; therefore the vertical wavelength for a phase velocity of 21 m/sec is 6 km. It is interesting to note that the vertical wavelength at these frequencies is almost independent of the horizontal size and depends essentially on phase velocity and on N. Vertical wavelength is shown as a function of altitude in Figure 9 for a phase velocity of 20 m/sec. If the phase velocity had been 30 m/sec as on May 15, 1954, the vertical scale size would have been 9 km at 80-km height.

Greenhow and Neufeld obtained observational data on the lower ionosphere using meteor data to obtain information about winds. They found

[3] The pressure microphone strongly suppresses the lower frequencies (its half-power period is about 20 minutes). Consequently, very large filter corrections had to be applied to the lowest frequencies. The low-frequency (or long-period) part of the curves is therefore doubtful. Since conservative values of the correction have been used in all cases, the actual energy at the lowest frequencies is probably larger (and perhaps considerably larger) than that indicated.

rms wind fluctuations of 25 m/sec. They defined time and length scales as the value at which their correlation functions became zero. They found a time scale of about 100 minutes, a horizontal scale size of 100 to 200 km, and a vertical scale size of 6 km. The apparent agreement of these figures with those which would be deduced from tropospheric waves may be deceptive. *Hines* [1960] pointed out that the length defined by the correlation function falling to zero is considerably smaller than the corresponding wavelength, and he estimated the actual vertical wavelength to be about 12 km. However, there is a considerable body of data from a variety of other sources which seems to support a vertical wavelength of about 6 km. This includes LF sounding data reported by *Helliwell* [1952], 2.28-Mc/s vertical incidence backscatter data reported by *Gardner and Pawsey* [1953], and rocket measurements of electron concentration reported by *Pfister and Ulwick* [1958].

Hargreaves [1961] obtained information about the lower ionosphere from 17-kc/s VLF amplitude data measured over a 1000-km path using spaced receivers. He reported an rms height fluctuation of the reflecting layer of about 1 km[4] and a mean drift velocity of 15 m/sec. His correlation functions are nearly exponential, and he therefore defined a length scale in terms of the separation distance at which the correlation fell to $e^{-1/2}$. The length scale of the ionospheric perturbations was found to be 23 km on the 1000-km path. *Harwood* [1953] used a similar experimental system at 16 kc/s, but his path length was only 100 km. This provided an approximately vertical incidence sounding system. His autocorrelation function falls to zero in 14 minutes in contrast with the Greenhow and Neufeld figure of 100 minutes.

It is seen that ionospheric data are in fairly good agreement with tropospheric gravity wave data. This is especially true if the higher frequencies in the tropospheric spectrum are removed by viscosity or by the growth of nonlinearity. Apparently Hines' suggestion that lower ionospheric irregularities may originate in the large energy processes of the troposphere should be seriously considered.

Generating mechanisms in the troposphere. There are three principal mechanisms for generating internal waves in the troposphere.

Internal gravity waves can be generated as standing waves in the lee of topographic features. Many mountains and ridges are famous for such effects. This type of generating mechanism has been considered in detail by many authors, and we shall not discuss it here.

Gravity waves are often caused by a traveling boundary between two types of air of different density. If the velocity of travel is of the proper magnitude relative to the height and intensity of the inversion and the slope of the boundary, such a traveling disturbance can cause an internal wave train to be generated in its wake. This type of tropospheric wave train is short, lasting less than 2 hours. The records are very regular and essentially sinusoidal in character. It is a fair-weather phenomenon, rarely associated with storm fronts. An example is shown in Figure 1.

Sometimes the oscillations last for many hours. The records are erratic and show complicated interference patterns. The records shown in Figure 4 are examples of this type of wave activity, and it is this type of record with which we are principally concerned when considering possible effects at ionospheric levels. This type of record is generally associated with tropospheric storms and synoptic scale features. On May 15 and November 10, precipitation fell in the San Diego area. However, in both cases the waves ceased (apparently owing to destruction of the inversion) before the rain began. On June 24, 1957, an area of weather south of San Clemente Island was tracked by radar westward during the morning of June 24. On this occasion nothing appeared on the synoptic weather map to indicate a storm off the coast, and the evidence indicates that a relatively small area of violent convective activity was responsible. Although the oscillations of long duration are usually generated by storms and frontal disturbances, the presence of a stable layer in the lower atmosphere is also required. The combination of an active generating mechanism in the presence of a stable layer in the troposphere is rather rare in southern California. However, this combination should occur often in the tropics and sub-

[4] It was pointed out to the author by J. F. Hargreaves that he observed a difference in amplitude between day and night (235 m vs. 990 m) which may be explained by the density difference between the day and night reflection heights. From the usually accepted values of 70 km and 90 km a factor of about 6 would be predicted.

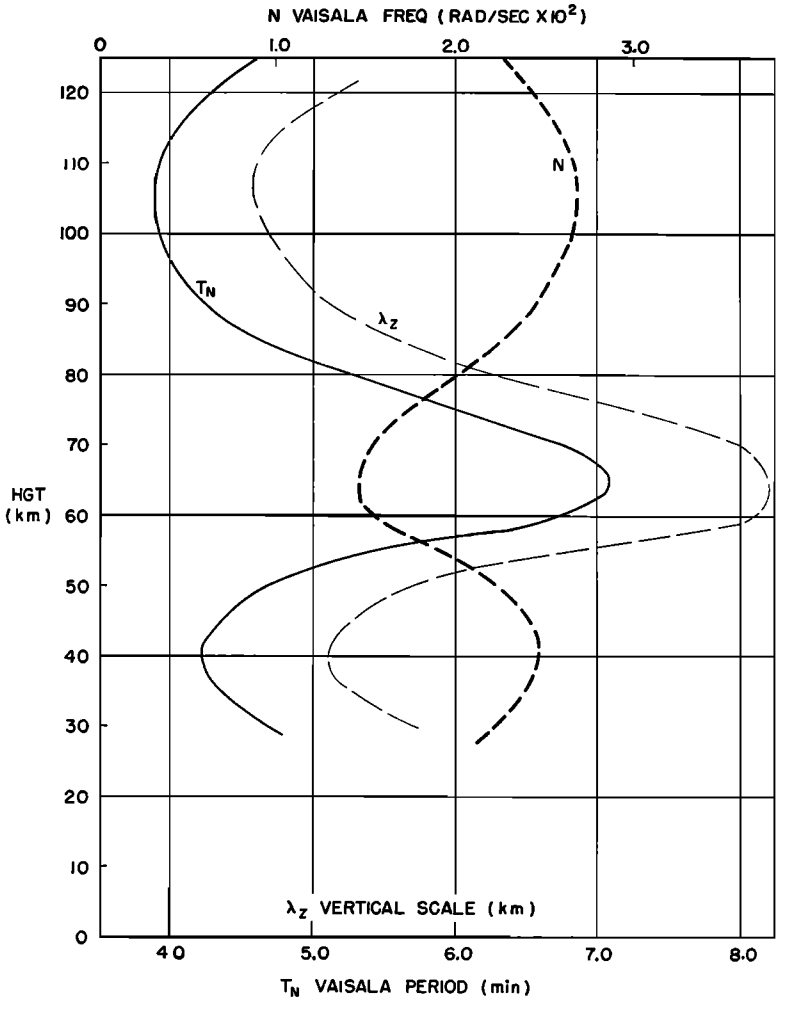

Fig. 9. Height distribution of Vaisala frequency and vertical wavelength assuming a phase velocity of 20 m/sec.

tropics, where active convection occurs in the presence of the trade-wind inversion. Unfortunately, the trade-wind inversion is usually so high that perturbations of the layer do not cause large fluctuations of wind or pressure at the surface. Also the signature of the waves is usually obscured by wind and pressure fluctuations due to local convection.

The perturbation equations. The linearized equations of motion, continuity, and energy for isentropic perturbations can be written as

$$\frac{D\mathbf{v}}{Dt} + \frac{1}{\rho_z}\nabla p - \frac{\rho}{\rho_z}\mathbf{g} = 0 \qquad (9)$$

$$\frac{\partial P}{\partial z} = -\rho_z g \qquad (10)$$

$$\mathrm{div}\,\mathbf{v} = -\frac{1}{\rho_z}\left(\frac{D\rho}{Dt} + w\frac{\partial \rho_z}{\partial z}\right) \qquad (11)$$

$$\frac{D\rho}{Dt} + w\frac{\partial \rho_z}{\partial z} = \frac{1}{c^2}\left(\frac{Dp}{Dt} + w\frac{\partial P}{\partial z}\right) \qquad (12)$$

where $\mathbf{v}$ is the velocity perturbation vector with components (u, v, w), ρ and p are the perturbed density and pressure, U and V are the undisturbed x and y components of velocity, ρ_z and P are the undisturbed density and pressure, and c

is the velocity of sound. D/Dt denotes the operation $\partial/\partial t + U(\partial/\partial x) + V(\partial/\partial y)$. Mean vertical velocity, friction, and Coriolis force have been assumed negligible for the frequencies and scale sizes we are considering.

It is convenient first to eliminate the density perturbation from the above set of equations. This is most easily done by taking the time derivative of the equation of motion in w and substituting from (11) and (12) to obtain

$$\frac{D^2w}{Dt^2} + \frac{1}{\rho_z}\left(\frac{\partial}{\partial z} + \frac{g}{c^2}\right)\frac{Dp}{Dt} - g\left(\frac{1}{\rho_z}\frac{\partial \rho_z}{\partial z} + \frac{g}{c^2}\right)w = 0 \qquad (13)$$

$$\frac{\partial u}{\partial x} + \frac{\partial v}{\partial y} + \left(\frac{\partial}{\partial z} - \frac{g}{c^2}\right)w + \frac{1}{\rho_z c^2}\frac{Dp}{Dt} = 0 \qquad (14)$$

Equations 13 and 14 combined with the horizontal equations of motion form a set of four linear homogeneous equations. If they are written in terms of the variables $(\rho_z^{1/2}u)$, $(\rho_z^{1/2}v)$, $(\rho_z^{1/2}w)$, $(\rho_z^{-1/2}p)$ and if $[\frac{1}{2}\ d(\ln\ \rho_z)/dz]$ and $[d(\ln\ \rho_z)\ dz + g/c^2]$ are assumed to be independent of z over the height interval considered, this set of equations has constant coefficients. Then the solution

$$\rho_z^{1/2}u,\ \rho_z^{1/2}v,\ \rho_z^{1/2}w,\ \rho_z^{-1/2}p = A_u,\ A_v,\ A_w,\ A_p \cdot \exp i(k_x x + k_y y \pm nz - \omega t) \qquad (15)$$

yields the propagation equation [see, for example, *Gossard and Munk*, 1954; *Eckart*, 1960] as

$$\nu^2 n^2 = (k_x^2 + k_y^2)(N^2 - \omega^2) + \frac{\nu^4}{c^2} - \left(\frac{1}{2\rho_z}\frac{\partial \rho_z}{\partial z}\right)^2\omega^2 \qquad (16)$$

where k_x, k_y, n are the components of the propagation vector, ν denotes $(\omega - Uk_x - Vk_y)$ and

$$N^2 = -g\left(\frac{1}{\rho_z}\frac{\partial \rho_z}{\partial z} + \frac{g}{c^2}\right) = g\frac{d}{dz}(\ln\ \theta) \qquad (17)$$

where N is in radians per second. If the medium is at rest and is isothermal, N^2 is given simply by $(\gamma - 1)\ (g/c)^2$, where γ is (here only) used as the ratio of the specific heats. Equation 16 then becomes Hines' equation 21. In an isothermal atmosphere the coefficients of the differential equations in the above variables are truly constant. In the more general case the coefficients are considered to be constant through fairly deep regions of the atmosphere, and the problem of a layered atmosphere can be treated. This is possible because the coefficients N and $[g/c^2 + (1/2\rho_z)(\partial\rho_z/\partial z)]$ which Eckart calls Γ depend principally on the height gradient of density rather than on density. In fact, the coefficients are considered to be constant over the whole depth of the troposphere by some authors [see, for example, *Queney*, 1947]. Equation 16 can be written in a presently more convenient form as

$$n^2 = \frac{k^2}{\nu^2}(N^2 - \nu^2) - \Gamma^2 \qquad (18)$$

where it has been assumed that $(\nu/k)^2$ is much smaller than c^2 and where k is the horizontal component of the propagation vector. For the horizontal phase velocities and stabilities with which we shall generally be concerned Γ may usually be neglected in the troposphere. Frequencies for which n is imaginary in a certain layer will be trapped by that layer.

From (18) the vertical group velocity V_z can be derived as

$$V_z = -\frac{\omega}{k}\left(\frac{\omega^2}{N^2}\right)\sqrt{\frac{N^2}{\omega^2} - \left(1 + \frac{\Gamma^2}{k^2}\right)} \qquad (19)$$

Equations 13 and 14 provide relations between pressure p and vertical velocity w as

$$\left(\frac{\partial}{\partial z} + \frac{g}{c^2}\right)\frac{Dp}{Dt} = -\rho_z(N^2 - \omega^2)w \qquad (20a)$$

$$\left(\frac{\partial}{\partial z} - \frac{g}{c^2}\right)w = -\frac{1}{\rho_z}\left(\frac{1}{c^2} - \frac{k^2}{\omega^2}\right)\frac{Dp}{Dt} \qquad (20b)$$

Equation 20*b* can be combined with equation 1 to yield a relation between horizontal velocity u and vertical velocity w as

$$k^2 u = \left(\frac{\partial}{\partial z} - \frac{g}{c^2}\right)\frac{\partial w}{\partial x} \qquad c \gg C \qquad (21)$$

Boundary conditions and frequency equation. The plane-wave solution for w in the κth layer of a multilayered atmosphere for propagation in the x, z plane is

$$w_\kappa = \rho_z^{-1/2}(A_\kappa e^{in_\kappa z} + B_\kappa e^{-in_\kappa z}) \cdot \exp i(kx - \omega t) \qquad (22)$$

The frequency equation is obtained by satisfying the dynamic and kinematic boundary conditions at the top of the κth layer in the form

$$w_\kappa = w_{\kappa+1}, \qquad \left(\frac{dp}{dt}\right)_\kappa = \left(\frac{dp}{dt}\right)_{\kappa+1}$$

$$w_0 = 0, \qquad w_\infty \neq \infty \tag{23}$$

The result for frequencies greater than N_3, N_1 in a three-layer atmosphere is given by Gossard and Munk as

$$n_2 \cot n_2 \Delta H = \frac{(S_3 - S_2 - \gamma_3)(S_1 - S_2 + \gamma_1 \coth \gamma_1 H) + {n_2}^2}{S_1 - S_3 + \gamma_3 + \gamma_1 \coth \gamma_1 H} \tag{24}$$

where $\gamma_{1,3}$ denotes $-i\, n_{1,3}$ and $-S$ is one-half the logarithmic derivative with height of ρ_z. The subscripts 1, 3 apply to layers below and above a stable layer of thickness ΔH with its base at H. S is generally quite unimportant for atmospheric density gradients and will be neglected. For a thin stable layer ($g\,\Delta H\,\Delta \ln \theta \ll (\omega/k)^2$), equation 24 becomes independent of ΔH and is

$$\left(\frac{\omega}{k}\right)^2 \cong \frac{gH\,\Delta \ln \theta}{\gamma_1 H \coth \gamma_1 H + \gamma_3 H} \tag{25}$$

This is the equation for a three-layer model in which the stable layer is thin compared with wavelength and is the same relation that holds for a model with a complete discontinuity in θ at H. This is a good approximation for most cases in southern California and is even better in areas where the tropospheric inversion is higher.

Equation 25 provides the basis for the present discussion of the untrapped frequencies. When γ_3 becomes imaginary, k becomes complex, and energy leaks into the upper atmosphere. In particular, if the lower layer is shallow and adiabatic ($\gamma_1 H = kH \ll 1.0$), equation 25 yields the curve of k_i as shown in Figure 6.

Energy density and energy flux. The most useful definition of vertical energy flux J_z [see *Eckart*, 1960] is expressed by equation 7.

Above the stable layer, equation 20*a* gives

$$\left(\frac{{N_3}^2}{\omega^2} - 1\right)\rho_z \omega w = -(n_3 - i\Gamma)p \tag{26}$$

For complex k, therefore,

$$J_z \cong -\rho_h \frac{\omega k_r}{|k|^2}\, {n_3}{w_h}^2 \tag{27}$$

where Γ^2 has been neglected for mathematical simplicity. Γ may be neglected whenever the square of the phase velocity is much less than N^2/Γ^2. N/Γ is approximately 100 m/sec for the cases considered, and the phase velocity never exceeds 30 m/sec. The error introduced is therefore less than 10 per cent, which is less than the ordinate uncertainty in the spectrum analysis.

Satisfying the dynamic and kinematic boundary conditions at the base of the (thin) stable layer, the vertical velocity w_h at the top of the layer is given by

$$w_h = w_H\left(\frac{\rho_H}{\rho_h}\right)^{1/2}\left(\frac{\gamma_1 \coth \gamma_1 H}{n_2} \cdot \sin (n_2\,\Delta H) + \cos (n_2\,\Delta H)\right) \tag{28}$$

Below H, the condition $w = 0$ at $z = 0$ requires that

$$w(z) = w_H\left(\frac{\rho_H}{\rho_z}\right)^{1/2} \frac{\sinh \gamma_1 z}{\sinh \gamma_1 H} \tag{29}$$

so that (20) gives

$$w_H = -i(\rho_H \rho_0)^{-1/2} \frac{k^2}{\omega} \frac{\sinh \gamma_1 H}{\gamma_1}\, p(0) \tag{30}$$

Equations 28 and 30 relate the surface pressure perturbation to the amplitude of the vertical velocity at h. The vertical displacement η is readily obtained by noting that w is the time derivative of η.

The total energy density ϵ in a gravity wave is the sum of the kinetic and thermobaric (potential) energies as given by equation 6. Above the stable layer, equation 21 shows that the total energy density at h is therefore given by

$$\epsilon \cong \rho_z {N_3}^2 {\eta_h}^2 \tag{31}$$

where terms in Γ^2 and Γn_i have been neglected. The average energy density and energy flux over a wave period is half the maximum values

which are given by equations 31 and 27. The average values are shown in the figures.

Data reduction and analysis. Digital sampling and computing procedures have been used throughout. Correlation and spectrum analyses have been discussed in detail elsewhere [*Munk, Snodgrass, and Tucker*, 1959; *Blackman and Tukey*, 1958]. The high frequencies in the pressure spectrum were measured with a barovariograph at U. S. Navy Electronics Laboratory. Usually the low frequencies were measured with an aneroid system at the Scripps Institution of Oceanography. However, because no aneroid record was available for June 24, 1957, the low-frequency data are from the barovariograph record on that day. The aneroid data were prefiltered using a numerical filter with low side bands to provide some compensation for the long-period nonstationarity in the absolute pressure record. The degrees of freedom in the spectrum analyses were 22 for the data on May 15, 1954, 18 for November 10, 1954, 31 for June 24, 1957 (A.M.), and 20 for June 24, 1957 (P.M.).

References

Blackman, R. B., and J. W. Tukey, *The Measurement of Power Spectra*, Dover Publications, New York, 199 pp., 1958.

Charney, J. G., and P. G. Drazin, Propagation of planetary-scale disturbances from the lower into the upper atmosphere, *J. Geophys. Research, 66*, 83–109, 1961.

Eckart, Carl, *Hydrodynamics of Oceans and Atmospheres*, Pergamon Press, New York, 1960.

Gardner, F. F., and J. L. Pawsey, Study of the ionospheric *D*-region using partial reflections, *J. Atmospheric and Terrest. Phys., 3*, 321–344, 1953.

Gossard, E. E., Spectra of atmospheric scalars, *J. Geophys. Research, 65*, 3339–3351, 1960.

Gossard, E. E., and W. H. Munk, On gravity waves in the atmosphere, *J. Meteorol., 11*, 259–269, 1954.

Greenhow, J. S., and E. L. Neufeld, Measurements of turbulence in the 80 to 100 km region from radio echo observations of meteors, *J. Geophys. Research, 64*, 2129–2133, 1959.

Hargreaves, J. K., Random fluctuations in very low frequency signals reflected obliquely from the ionosphere, *J. Atmospheric and Terrest. Phys., 20*, 155–166, 1961.

Harwood, J., Spaced-receiver experiments on radio waves of 19 km wavelength, *Proc. Inst. Elec. Engrs., London, 101*, 183–186. 1953.

Helliwell, R. A., Sporadic *E* stratification and correlation with low frequency soundings, *IRE Trans. on PGAP, 3*, 140–142, 1952.

Hines, C. O., Internal atmospheric gravity waves at ionospheric heights. *Can. J. Phys., 38*, 1441–1481, 1960.

Johnson, C. R., and J. R. Chiles, The NEL T21 microbaragraphic recording system, *U. S. Navy Electronics Lab. Rept. 773*, 68 pp., 1957.

Munk, W. H., F. E. Snodgrass, and M. J. Tucker, Spectra of low-frequency ocean waves, *Bull. Scripps Inst. Oceanog. Univ. Calif., 7*, 283–361, 1959.

Pfister, W., and J. C. Ulwick, The analysis of rocket experiments in terms of electron-density distributions, *J. Geophys. Research, 63*, 315–333, 1958.

Queney, P., Theory of perturbations in stratified currents with applications to air flow over mountain barriers, *Univ. Chicago Misc. Rept. 23*, 81 pp., 1947.

U. S. Air Force, *Handbook of Geophysics*, revised ed., Air Force Cambridge Research Center, Bedford, Mass., 1960.

(Manuscript received September 21, 1961; revised November 3, 1961.)